One pot synthesis of PbS/Cu$_2$S core-shell nanoparticles and their optical properties

T. Serrano and I. Gómez*
Universidad Autónoma de Nuevo León,
Facultad de Ciencias Químicas, Laboratorio de Materiales I,
San Nicolás de los Garza, Nuevo León, México,
*Phone (+52) 81-83294000 ext. 6362, Fax (+52) 81-83765375,
e-mail: maria.gomezd@uanl.edu.mx

The synthesis of PbS/Cu$_2$S core-shell nanoparticles with emission on the visible range and with improved luminescence properties was carried out by the colloidal solution-phase growth method by using simple stabilizers such as trisodium citrate and 3-mercaptopropionic acid. The core shell arrangement for particles with different crystalline structure was achieved, in addition this is the first report related to the synthesis PbS/Cu$_2$S core-shell system. The data obtained from absorption spectra, PL spectra, and HRTEM image provided direct proof of the formation of PbS core with size around 11 nm and Cu$_2$S shell of 5 nm thickness. According to the UV-vis absorption and PL spectrum, the optical characteristics observed in the synthesized material correspond to a PbS/Cu$_2$S system that has a higher confinement effect than the pure PbS nanoparticles. The QY was improved in 15 % from PbS to PbS/Cu$_2$S nanoparticles. The estimated band (HOMO-LUMO) alignment determined by CV measurements corresponds to a type-I core shell arrangement.

Keywords: Semiconductors; core-shell; PbS; Cu$_2$S; synthesis.

PACS: 81.07.-b; 42.70.-a; 61.46.Hk

1. Introduction

The synthesis and characterization of nanoparticles of semi-conducting metal sulfide has been an intense field of research due to the interesting properties and potential applications of those compounds [1-5]. Among sulfides, lead sulfide (PbS) and copper (I) sulfide (Cu$_2$S) have been investigated along the time because of their optical and electronic properties, what make them suitable for photovoltaic devices [6-7].

PbS nanoparticles are very interesting system in that their particle shapes and sizes can be varied by controlling the synthesis conditions [8-11]. The Bohr radius of PbS is large (18 nm) and its bulk band gap is small (0.41 eV), 12 therefore, it is relatively easy to prepare particles with size smaller than the Bohr radius that show strong quantum confinement effects. Their main advantage, those particles still absorb in the visible part of the spectrum. In addition, PbS and PbSe nanoparticles present the multiple exciton generation phenomena [13-14] and they can produce n excitons for each absorbed photon possessing an energy of at least n multiples of the band gap energy (Eg), where n is an integer number [15]. This phenomenon is very interesting for solar cell devices.

Cu$_2$S is a p-type semiconductor in which copper atom vacancies act as acceptors,[16] and it has been frequently investigated due to its attractive optical and electrical properties [17-18]. However, copper sulfide has a fairly complex crystal chemistry generally represented as Cu$_x$S (2> x >1), because there are numerous stable and metastable species, which have various compositions ranging between Cu$_2$S (Chalcocite) and CuS (Covellite) [18-19] in which Cu$_2$S is not as stable in solution as the CuS [20]. It has been demonstrated that Cu$_2$S is a good compound for active light-absorbing component. An example is the synthesis of colloidal Cu$_2$S nanocrystals and it application as an active light-absorbing compound in combination with CdS nanorods in order to produce a solar cell with 1.6% power conversion efficiency and stability over a four month testing period [21].

Cu$_2$S-PbS heterojunction has been investigated recently due to its optical and photothermal activation. A strong near infrared (NIR) absorption in the spectrum of the Cu$_2$S–PbS heteronanostructures besides the Cu$_2$S spectrum was found and it was attributed to the excitonic absorption of PbS nanocrystals. This fact suggest that in this type of heterostructure the photon can be absorbed by both of the two components (PbS-Cu$_2$S), making them a really interesting system for photovoltaic applications [22].

An important strategy to improve the nanoparticles efficiency and stability against photo-oxidation of various types of semiconductor is their surface passivation with the growth of a second semiconductor shell, resulting in core-shell system. Scientists have studied several methods in order to grow core shell chalcogenide nanoparticles with an emphasis on better control of size, shape, and size distribution [23]. We propose that a material that contains PbS and Cu$_2$S will enhance both materials optical properties when it is arranged in the core-shell structure.

The aim of this paper is to show the results on the synthesis and characterization of the PbS/Cu$_2$S system. To the best of our knowledge, this is the first time PbS and Cu$_2$S have been synthesized via a colloidal solution-phase growth method in the core-shell arrangement.

2. Experimental

PbS nanoparticles synthesis: reactants used in this work were all obtained from Aldrich with purities above 99.0%, therefore no further purification was required. All solutions were prepared using distilled water previously degassed under N$_2$ flow. PbS nanoparticles were prepared with a 1 mL solution of thioacetamide (CH$_3$CSNH$_2$, TAA) and of lead(II) chloride (PbCl$_2$) both 30 mM. Previously, 50 mL of sodium citrate (C$_6$H$_5$O$_7$Na$_3$·2H$_2$O) 3.0 mM where prepared and the CH$_3$CSNH$_2$ and PbCl$_2$ were added to the sodium citrate solution. Then the pH was varied from 6 to 9 for the different experiments. The mixtures were placed under reflux conditions for 30 min to obtain the dispersed nanoparticles.

PbS/Cu$_2$S nanoparticles synthesis: The PbS nanoparticles previously prepared were used without any purification. 0.50 g of 3-mercaptopropionic acid (MPA, C$_3$H$_6$O$_2$S) were added to the reaction vessel and the pH was adjusted to 8. The mixture was reacted during 30 min under reflux conditions and it was degassed with N$_2$ flux. Then, a solution of copper chloride (CuCl$_2$·2H$_2$O) was added drop wise to the reaction vessel, with a flow rate of 0.30 mL/min. After the addition of the CuCl$_2$ solution, the mixture was reacted during 6 hours under reflux conditions.

The synthesized material was studied with different techniques. The size and dispersion of the particles were determined by ultraviolet-visible (UV-Vis), photoluminescence (PL) and quantum yield (QY), Dynamic Ligth Scattering (DSL) method and X-ray diffraction (XRD) with copper radiation ($\lambda = 0.15418$ nm). UV-vis absorption spectra were obtained using a Perkin Elmer UV-vis Lambda 12 spectrophotometer. The cyclic voltammetry (CV) were carried out with the PbS and PbS/Cu$_2$S as a casting film on a Al foil electrode in the presence of 0.1 M NaClO4 in acetonitrile at a scan rate of 50 mV/s. The counter electrode is a Pt wire and the reference electrode was Ag/AgCl in saturated KCl. All measurements were taken using an Epsilon (BAS) potentiostat. Fluorescence experiments were performed using a Perkin Elmer PL Lambda 12 spectrofluorimeter using a wavelength of excitation of 330 nm. The QY was obtained from PL measurements using Rhodamine 6G as reference (0.95 in ethanol). All optical measurements were performed at room temperature under ambient conditions. Dynamic Ligth Scattering (DSL) analysis were performed on the colloidal synthesis medium with a particle size analyzer Zetatrac from Microtrac Samples were precipitated with i-propanol-acetone for XRD characterization. The XRD patterns were obtained from a Siemens D5000 Cu Kα ($\lambda = 1.5418$Å) diffractometer from 5 to 90° 2θ with a 0.05° 2θ step and 2 s per step. DSL analyses were performed with a Zetatrac NPA 152 from Microtrac. SEM images were obtained using a FE-SEM JEOL 6701 and HRTEM analysis was performed using a FEI Titan 80-300 microscope.

3. Results and Discussion

The synthesis of PbS nanoparticles was performed using TAA and PbCl$_2$ as precursors. As stabilizer we chose sodium citrate, due to its low toxicity and good stabilization properties previously studied by our group for CdS nanoparticles [24]. The formation of a dark brown solution was observed indicating the presence of PbS nanoparticles, Scheme 1 shows the synthesis process. PbS nanoparticles were used without any purification to the synthesis of the PbS/Cu$_2$S
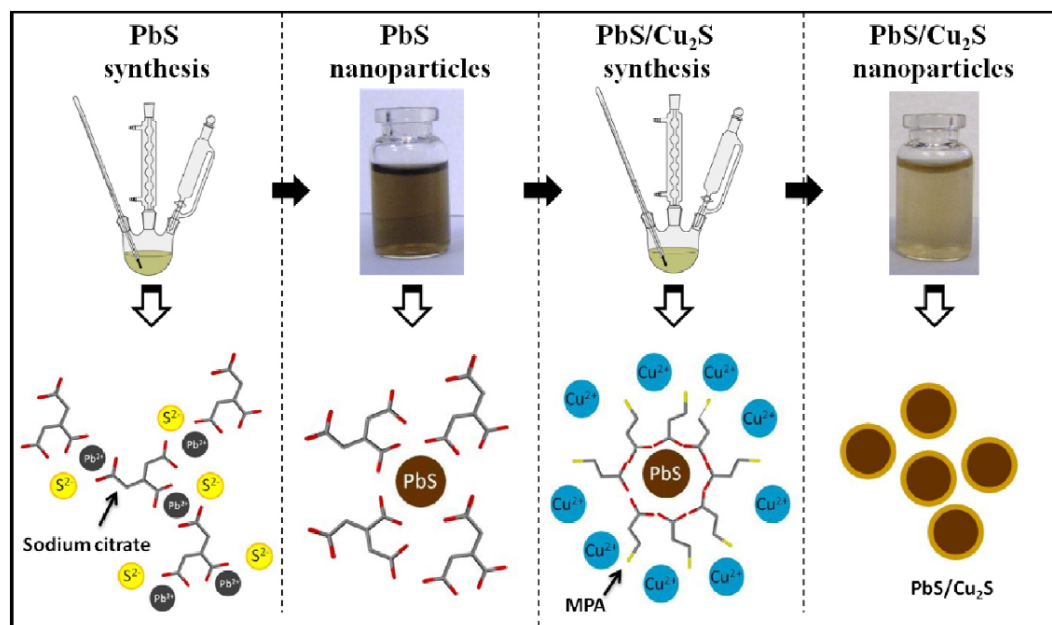
SCHEME 1. Synthesis of PbS/Cu$_2$S core-shell system by the solution-phase growth method.

core-shell system. For that MPA was added to the reaction vessel as stabilizer and sulfur source, then a solution of CuCl$_2$·2H$_2$O was added drop wise for the formation of the desired system.

After the addition of the CuCl$_2$·2H$_2$O solution, the sample presented a change in color and the solubility of the system decreases until the precipitation of gold-brow particles (see Scheme 1). MPA is an organic carboxylic acid with a thiol functional group (-SH) which may act at the same as a sulfur source, reducing agent for the copper (II) ions and capping agent. Those properties make MPA an ideal candidate for the Cu$_2$S stabilization. The addition of MPA to the reaction mixture help to stabilize the PbS nanoparticles by capping its surface, then the copper (II) ions surround the PbS-MPA and they are reduced to the formation of copper (I) ions. The thiol group lead to the presence of sulfur ions which react with the copper (I) ions linked to the PbS surface for the formation of the Cu$_2$S shell. This mechanism corresponds to the growth seed method, where the core acts as a seed and the nuclei of the shell material growth covering the surface to the formation of the shell. The presence of MPA molecules onto the surface of the PbS/Cu$_2$S nanoparticles helps to the chemical stabilization in solution as well as in atmospheric conditions. The synthesized nanoparticles are stables in aqueous degassed solution or in non-oxidative conditions; they are remain stables in air for one week.

It is well known that the absorption edge is blue-shifted when the size of semiconductor nanoparticles decreases [25]. For PbS nanoparticles, it was reported that the UV-vis absorption edge shows a marked blue-shift from that of the bulk PbS crystals which is expected around 1200 nm.[19] UV-Vis spectroscopy was applied to obtain information about the light interaction of the PbS nanoparticles. Figure1a and 1b show the absorption spectra of the PbS nanoparticles prepared at different pH and the absorption and luminescence spectra for the PbS synthesized at pH=8. The absorption of the PbS nanoparticles starts around 800 nm and it increases with decreasing the wavelength, three salient shoulders are present around 600, 400, and 300 nm and they are attributes to exciton peaks of 1s$_e$-1s$_h$, 1s$_e$-1p$_h$, and 1p$_e$-1p$_h$ transitions, respectively [26-27] due to quantum confinement. The luminescence spectrum for PbS nanoparticles at pH=8 presents an emission peak centered at 700 nm with a FWMH of 24 nm, which correspond to the previously discussed absorption on the UV-Vis spectra for the 1se-1sh exciton transition. The QY determination was performed on the PbS nanoparticles by using Rhodamine 6G as reference, the QY value was estimated to be 0.63.
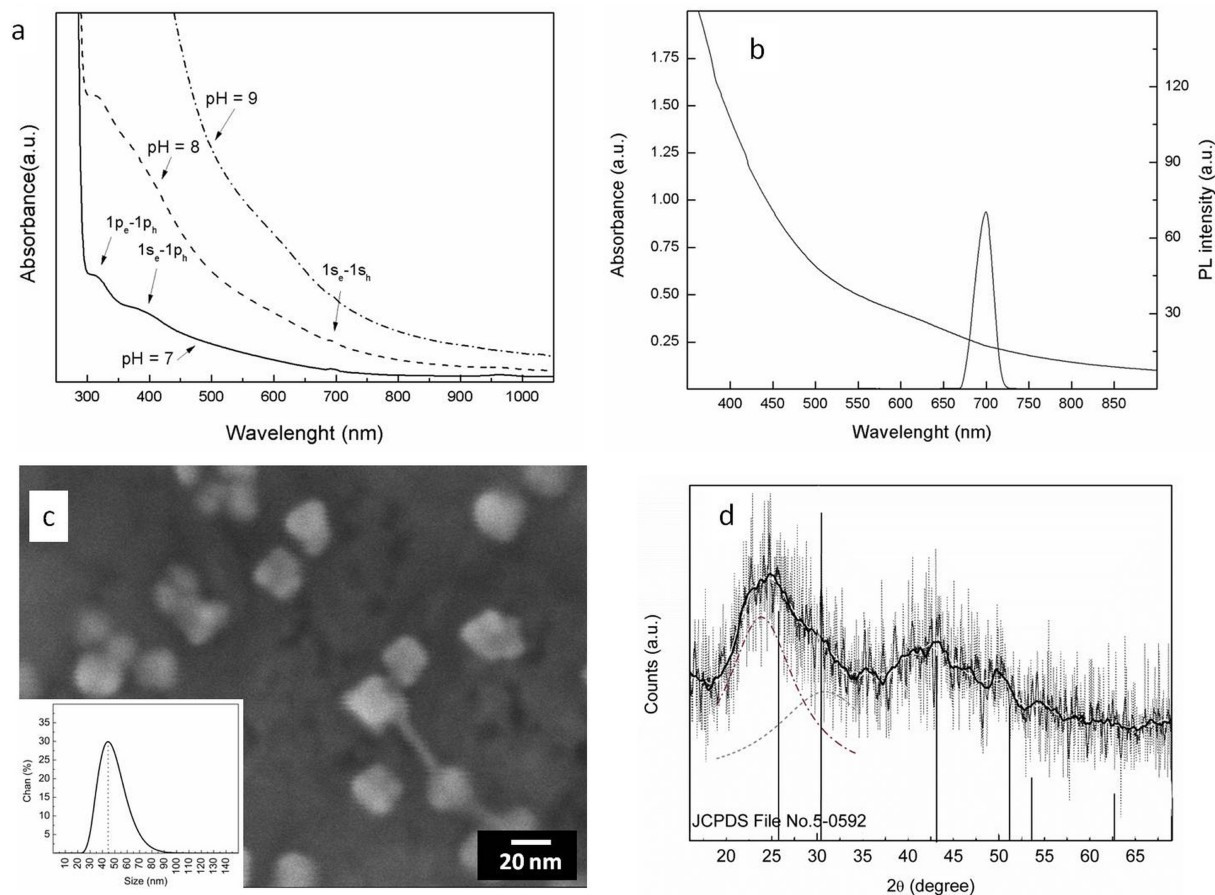

FIGURE 1. a) Absorption spectra for PbS nanoparticles synthesized at different pH. b) absorption and PL spectra, c) SEM images and particles size distribution (inserted figure) and d) XRD pattern of PbS nanoparticles synthesized at pH = 8.

For the PbS nanocrystals prepared in solution, the optical band gap values of 1.80, 1.55 and 1.37 eV were calculated from the UV-vis absorption for the experiments at pH 7, 8 and 9, respectively. It is clear that the pH of the reaction mixture have an important influence in the particle size and the optical characteristics of the material. It can be assumed that particles synthesized at pH=7 present stronger quantum effects, however the chemical stability of those particles is lower than the particles synthesized at pH=8 and the higher amount of defects present on the surface of the particles synthesized at pH=7, may act as exiton traps In this case, it was decided to work at pH=8 for the synthesis of the core-shell structure. FESEM analysis performed on PbS nanoparticles (Fig. 1c) reveled the formation nanoparticles with spherical morphology and average size of 12 nm, the formation of agglomerates of four particles in a quadrangular arrangement, with sizes around 40 nm was also observed. Figure 1d shows the particle size distribution by DSL analysis of the PbS nanoparticles. The distribution is centered on 45 nm corresponding to the size of the agglomerates observed by FESEM.

X-ray diffraction spectrum of PbS processed by colloidal method at pH=8 (Fig. 1d) was fitted in order to determine the contribution and position of each signal. Signals centered at 23.8° and 31.2° , were found and they correspond to the 111 and 200 reflections. In addition, reflection at 43.3°, 49.7° and 54.4° are present and they correspond to the 220, 311 and 222 reflections, respectively. The pattern was compared to the galena diffraction pattern (JCPDS File No.5-0592) and it corresponds to the expected face-centered cubic structure of rock salt system, with cell parameter of 5.95 Å.

After the characterization of the PbS nanoparticles, the Cu$_2$S shell was overgrowth. The concentration of the CuCl$_2$ solution was adjusted to have different ratios of PbS:Cu^{2+}. Figure 2a corresponds to the synthesis of 1:1 PbS:Cu^{2+} ratio, with the formation of PbS cubes and Cu$_{1.8}$S flakes. The formation of a Cu$_{1.8}$S phase is related to the insufficient amount of MPA for the complete reduction of the total amount of copper (II) ions. The synthesis of 1:0.5 PbS:Cu^{2+} ratio produced the formation of a mixed material of PbS/Cu$_2$S with a flower-like morphology of 3 μm length, the PbS nanoparticles act as seeds for the growth of Cu$_2$S leaves to the formation of the PbS-Cu$_2$S flower-like structure. Nevertheless, this compound did not present interesting optical properties, the UV-Vis analysis of this compound (not showed in the paper) show the two characteristic signals for PbS and Cu$_2$S, not NIR signal (characteristic of CuS nanoparticles) was detected. The synthesis of the 1:0.2 PbS:Cu^{2+} ratio were the formation agglomerated of PbS spherical nanoparticles embedded in a Cu$_2$S matrix. The morphology changes due to the different concentrations of copper (II) ions are mainly attributed to the chemical solubility of the compounds, where Cu$_2$S is a material with a lower chemical solubility compared to PbS. The addition of copper (II) ions to the previously prepared PbS nanoparticles leads to the immediate precipitation of the Cu$_2$S nanoparticles. As the growth of the desired shell

is a diffusive process, the high speed rate of precipitation do not give enough time to the system to be arrange in a core-shell structure, leading to the separation of the two materials. Figures 2c and 2d shows the 1:0.2 and 1:0.1 PbS:Cu$_2$S, respectively. It can be observed that the formation of the PbS/Cu$_2$S desired material in the core-shell arrangement was achieved due to several factors: the concentration ratio, the Cu^{2+} addition rate and the total reaction time. HRTEM, showed in Figs. 2e and 2f, were employed to study the morphology of PbS/Cu$_2$S. It can be seen that the nanoparticles are basically spherical shaped with a total diameter of around 20 nm. The PbS core present a size around 11 nm, with an interplanar distance characteristic for the PbS system in the cubic face centered structure [7], this fact is in agreement with the observations discussed in the XRD analysis. The shell presents a thickness of around 5 nm, with an interplanar distance of 3.0 Å, corresponding to the (101) lattice plane of hexagonal Cu$_2$S [6]. This analysis confirms the presence of the material in the desired core-shell configuration. The presence of Cu$_2$S nanoparticles of 5nm surrounding the core-shell structure supports the suggested growth method of the shell, previously discussed.

Figure 3 shows the UV-Vis and PL spectra for PbS and PbS/Cu$_2$S nanoparticles were the main characteristics of the absorption spectra of PbS nanoparticles are present for the PbS/Cu$_2$S nanoparticles and the exiton signals could still be appreciated. The absorption wavelength for the PbS/Cu$_2$S system was significantly blue shifted from the one of PbS due to the addition of the Cu$_2$S shell. This can be attributed to the absorption region of the Cu$_2$S which is regularly observed in the visible light range. This interaction provides a material with the good optical properties of the PbS nanoparticles in the visible range instead of the NIR range, what makes a good advance for the development of photovoltaic devices. In addition, the absence of peaks at NIR, characteristics of CuS particles in the PbS/Cu$_2$S spectrum indicates the formation of the desired material with high purity (Cu$_2$S). The optical band gap for the core-shell nanoparticles was calculated to be 1.8 eV (see Table I). This value is larger than the Eg(bulk) of Cu$_2$S (1.21 eV) [17] and it gives an idea about the quantum confinement of the system, due to the core-shell structure. The main optical modification is observed on the PL spectra, were the intensity of the PL is dramatically increased and the peak is slightly shifted to 695 nm and it present a FWMH of 28 nm. In the same way as PbS nanoparticles, the QY determination was performed on the PbS/Cu2S nanoparticles by using Rhodamine 6G as reference, the QY value was estimated to be 0.78.

This blue shift has been observed in some other PbS core-shell system. Kumar and Jakhmola [28], reported the PbS/ZnS nanoparticles system, in order to study the PbS covered with a semiconductor of larger band-gap. The reported that the addiction of ZnS shell in low concentration (shell thickness and covered core area) did not exhibit any special spectral change, nonindicating the interaction between both materials; however, at high concentration of ZnS into the
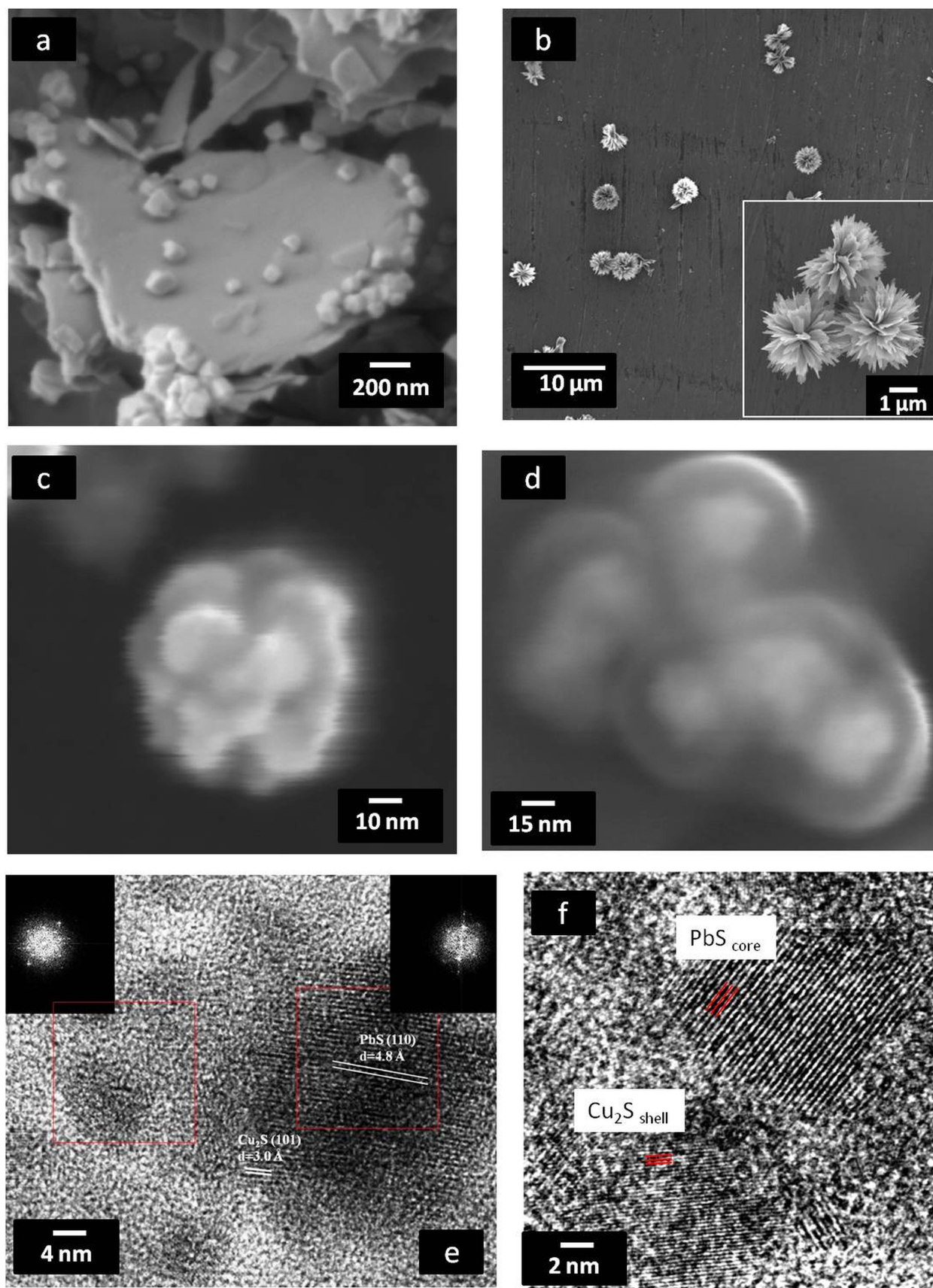
FIGURE 2. SEM images of PbS-Cu$_2$S nanoparticles synthesized with a)1:1, b) 1:0.5, c) 1: 0.2 and d) 1:0.1 ratios of PbS:Cu^{2+} precursors, e) and f) HR-TEM images of PbS-Cu$_2$S nanoparticles synthesized 1:0.1 ratio of PbS:Cu^{2+} precursors.

core-shell system, the absorption coefficient of the composite particles decreases to wavelength in the range of 350-500 nm, contrary to the original PbS that absorbs in the 450-600 range, observing a blue shift of the absorption signal. In the same paper, the author describes the ZnS/PbS system, where contrary to the observed in the PbS/ZnS system, the absorption spectra of the material, presents a red shift as the concentration of PbS increases. PL spectra from the same paper, revels a blue shift for the core-shell system compared to the original PbS nanoparticles where the relaxation dynamics of charge carries is influenced by the passivation of the surface what enhances the life time and it enlarges the QY values. Kovalenco *et al.* [29] reported the synthesis of the PbS/CdS system, where they observed the original absorption of PbS nanoparticles at 1350 nm and the absorption of the PbS/CdS system at 1190 nm (Fig. 1 supplementary information), observing a blue shift of the absorption wavelength due to the addition of a shell semiconductor with larger band-gap the core. They also observed a shifting of PL peak position to shorter wavelengths, it was explained by the formation of an increasingly thick CdS shell resulting from sacrificial replacement of lead with cadmium, which would reduce the size of the pure PbS core and result in bluer than predicted emission. This phenomena was observed on system that contain PbS and PbSe nanoparticles and it have been attributed to the confinement of the PbS (or PbSe) nanoparticles. Even when due to the size enlargement the absorption spectra is expected to be red shifted, heterostructures with a small conduction-band offset and a large valence-band offset suggest that electron wave functions extend into the CdS shell while holes are efficiently confined in the PbS core, reducing the electron-hole overlap, what produces the blue shift observed in most of this type of system.

The Eg of the nanoparticles synthesized in this work, was calculated by means of electrochemical method. Cycling voltammetry (CV) measurements were used for the determination of band structure parameters. It is a dynamic electrochemical method, where current-potential curves are record-
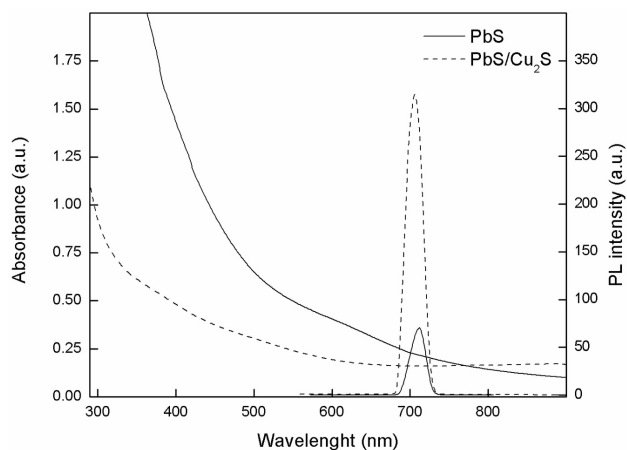
ed at well-defined scan rates. The measured oxidation potential of an electroactive substance correlates directly with the ionization potential I_p and the reduction potential with the electron affinity E_a As long as the vacuum level potentials of the common reference electrodes are known, the band edge positions of electroactive materials can be estimated [30]. This kind of information cannot be determined from UV/vis spectroscopy. The conduction band edge (e_1, LUMO), valence band edge (h_1, HOMO), and gap of quasi-particle calculations by means of CV have been described by different research groups [30-32]. The electron transfer with quantum confined nanoparticles is mediated through e_1 and h_1, which are manifested as respective cathodic and anodic peaks in the CV measurements.

In the present investigation, the CV measurements were carried out on the PbS and PbS/Cu₂S core/shell synthesized materials. Thus, the charge transfer can be viewed as a formation of the non-interacting electronhole pair, the potential difference between cathodic and anodic peaks is correlated to the single particle or quasi-particle gap. Figure 4a shows the typical CV recorded for the dispersion of PbS and PbS/Cu₂S nanoparticles. The prominent, cathodic and anodic peaks were observed at ca. -0.60 V and 1.00 V. The samples an
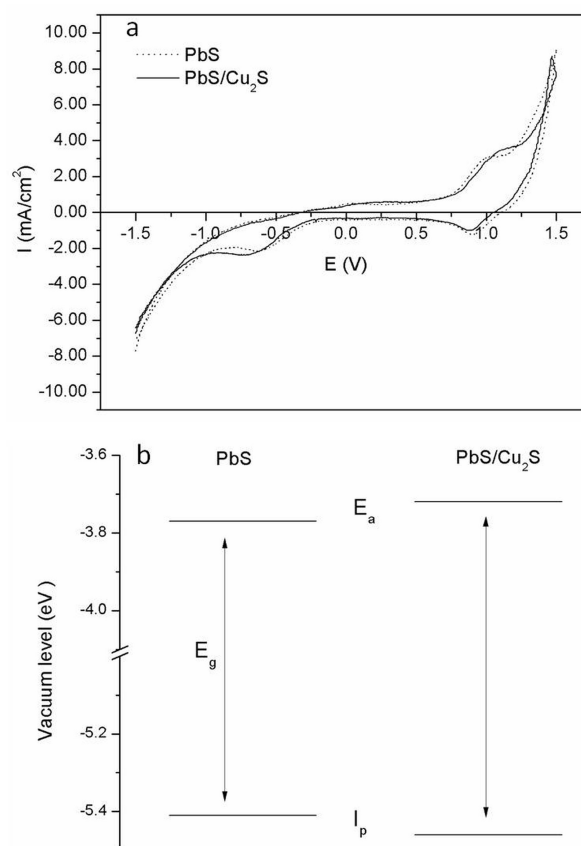
FIGURE 4. a) Cycling Voltammetry of PbS and PbS/Cu₂S nanoparticles on Al electrode for the determination of the quasi-particle gap values and b) Schematic diagram of the electrochemically determined ionization potentials I_p and electron affinities E_a of PbS and PbS/Cu₂S nanoparticles.

FIGURE 3. Absorption and PL spectra of PbS nanoparticles and PbS/Cu₂S core-shell nanoparticles.

TABLE I. Band Structure Parameters of PbS/Cu2s nanoparticles, obtained from UV-Vis spectroscopy and Cyclic Voltammetry.

Material	UV-Vis	Cycling Voltammetry		
	Optic band gap	valence band edge	conduction band edge	Quasiparticle gap
	(eV)	h_1 (eV)	e_1 (eV)	(eV)
PbS	1.55	-5.41	-3.77	1.63
PbS/Cu$_2$S	1.80	-5.46	-3.72	1.74

extra anodic peak at ca. 0.89 V, which is found to be complementary to the cathodic signal and it indicates that the reduction of the nanoparticles forms a relatively stable anion radical in a given time frame and the solvent system [33]. This peak has been observed for nanoparticles that present strong light interactions, especially for those with dramatically increased luminescent properties. After more, in the CV measurements the cathodic and anodic peaks shift to more negative and positive potentials, respectively for the PbS/Cu$_2$S compare with the PbS system. This phenomenon is observed for nanoparticles that present strong quantum confinement, as this shift increases the quantum confinement becomes more important for the nanoparticles behavior. In the case of the studied materials, it is clear that the PbS/Cu$_2$S nanoparticles present stronger quantum phenomena than the PbS nanoparticles, what support that the addition of a Cu$_2$S layer helps to stabilize the PbS core.

In order to estimate the ionization potential I_p and the electron affinity E_a of the nanoparticles from their oxidation and reduction waves it is necessary to relate the electrochemical potentials to the vacuum level. Such an estimation has been done for electrochemical measurements of conducting polymers[34-35] and semiconductor nanoparticles [32,36]. It is expected that

$$I_p = -(E_{\text{ox}} + 4.4) \text{ eV} \tag{1}$$

$$E_a = -(E_{\text{red}} + 4.4) \text{ eV} \tag{2}$$

where I_p is the ionization potential, E_a is electron affinity, E_{ox} is the potential of oxidation, and E_{red} is the potential of reduction. The 4.4 eV constant in the relation between Ip, Ea, and redox potentials arises from the difference in gas phase ionization potentials and electrochemical oxidation potentials of solid films and the solid state polarization energy, it means the vacuum level potentials of the reference electrode [37] Table I outlines the Ip and Ea values found for PbS and PbS/Cu$_2$S nanoparticles, as well as the E_g values determined by the optical and electrochemical method. In addition, Fig. 4b depicts schematically the electrochemically determined I_p and E_a values on the vacuum level calculated from Eqs. (1) and (2). It was found that the ΔE values are in good agreement with the optical measurements. The general tendency of the I_p and E_a values is in good agreement with the expectations based on the quantum confinement effect and predicted theoretically [32].

Depending on the Eg and the relative position of electronic energy levels of the involved semiconductors, the shell can have different functions in the core-shell system. In type-I core-shell structures, the shell is used to passivate the surface of the core with the goal to improve its optical properties. The shell physically separates the surface of the core from the surrounding medium producing modifying the sensitivity of the optical properties to changes in the local environment of the nanoparticles, induced by the presence of oxygen or water molecules, and in this case PbS photodissolution [23]. With respect to core particles, core-shell systems exhibit generally enhanced stability against photodegradation. At the same time, shell growth reduces the number of surface dangling bonds, which can act as trap states for charge carriers what induced an enlargement of the quantum yield. In this case, the addition of the Cu$_2$S shell induces the passivation of the PbS core, leading to the optical enhancement observed by the absorption and PL spectra.

As previously mentioned, QY determination was performed on the PbS and Cu$_2$S nanoparticles, for PbS nanoparticles the QY was determined to be 0.63 (or 63%) what is in the range of reported PbS nanoparticles with high confinement. The QY for PbS/Cu$_2$S was calculated to be 0.78 (78%) what makes an increment of 15 percent units in the QY. This behavior confirms the enhancement of the optical properties and confirms the core confinement due to the passivation with the shell, what is characteristic of a type-I core shell structure. The result obtained by UV-Vis, PL spectroscopy, QY determination and the electrochemical measurements, correspond to the description of a type-I core-shell system where the core band values, I_p and E_a, are included in to the shell band values. It allows producing a material in which the growth of the shell reduces the surface dangling bonds, and significantly improves the fluorescence of the system. This observation is attributed to a partial leakage of the exciton into the shell material.

4. Conclusion

In summary, this work describes the synthesis of PbS/Cu$_2$S core-shell nanoparticles with emission on the visible range and with improved luminescence properties. The synthesis was carried out by the colloidal solution-phase growth method by using simple stabilizers such as sodium citrate and 3-mercaptopropionic acid and the core shell arrangement for particles with different crystalline structure was achieved. This is the first report related to the synthesis PbS/Cu$_2$S core-shell system, to the best of our knowledge, the data from

absorption spectra, UV-vis, PL spectra, and TEM provided direct proof of the formation of PbS core with size around 11 nm and Cu$_2$S shell of 5 nm thickness. According to the UV-vis absorption, electrochemical measurements and PL spectrum, the optical characteristics observed in the synthesized material correspond to a PbS/Cu$_2$S system that has a higher confinement effect than the pure PbS nanoparticles, this fact was confirmed by the QY measurement for PbS (0.63) and PbS/Cu$_2$S (0.78). The band alignment and band gap of the material was determined by CV and it corresponds to a type-I core shell arrangement.

Acknowledgments

1. C. B. Murray, C. R. Kagan and M. G. Bawendi, *Ann Rev Mater Sci.* **30** (2000) 545–610.

2. J. T. Hu, L. S. Li, W. D. Yang, L. W. Manna, L. Wang and A. P. Alivisatos, *Science.* **292** (2001) 2060–2063.

3. R. Heath, P. J. Kuekes, G. S. Snider and R. S. Williams, *Science.* **280** (1998) 1716–172.

4. W. U. Huynh, J. J. Dittmer and A. P. Alivisatos, *Science.* **295** (2002) 2425–2427.

5. H. H. Kung and M. C. Kung, *Catalysis Today.* **97** (2009) 219–224.

6. S. Li, H. Z. Wang, W. W. Xu, H. L. Si, X. J. Tao, S. Lou, Z. Du and S. L. Li, *Journal of Colloid and Interface Science.* **330** (2009) 483–487.

7. J.C. Querejeta-Fernandez, *et al.*, *ACSNano.* **6** (2012) 3800–3812.

8. J.D. Patel, F. Mighri, and A. Ajji, *Materials Letters*, **74** (2012) 183–186

9. C. Ratanatawanate, C. Xiong, and K.J. Balkus, *ACSNano* **2** (2008) 1682–1688.

10. D. Kumar G. Agarwal, B. Tripathi, D. Vyas, and D. Kulshrestha, *Journal of Alloys and Compounds* **484** (2009) 463–466.

11. M. Rajamathi, R. Seshadri, *Current Opinion in Solid State and Materials Science*, **6** (2002) 337–345.

12. M. Neo, N. Venkatram, G.S. Li, W.S. Chin, and W. Ji, *J. Phys. Chem. C* **114** (2010) 18037–18044.

13. H.W. Hillhouse, and M.C. Beard, *Current Opinion in Colloid & Interface Science.* **14** (2009) 245–259.

14. V.P. Singh, R.S. Singh, and K.E. Sampson, *Nanostructured Materials for Solar Energy Conversion* (T. Soga. Elsevier B.V. 2006).

15. A.J. Nozik *Phys E Low-Dimens Syst Nanostruct* **14** (2002) 115–20.

16. K. Okamoto and S. Kawai, *Jpn J Appl Phys.* **8** (1973) 1130–1138.

17. C. Nascu, I. Pop, V. Ionescu, E. Indrea and I. Bratu, *Mater Lett.* **32** (1997) 73–77.

18. H. S. Randhawa, R. F. Bunshan, D. G. Brock and B. M. Basol, *Solar Energy Mater.* **6** (1982) 445–453.

19. J. J. Loferski, J. Shewchun, S. D. Mittleman, E. A. Demeo, R. Arnott, H. L. Hwang and R. Beaulieu, *Solar Energy Mater.* **1** (1979) 157–169.

20. E. Saunders, A. Ghezelbash, D. M. Smilgies, M. B. Sigman and B. A. Korgel, *Nano Lett.* **6** (2006) 2959–2963.

21. Y. Wu, C.Wadia, W. Ma, B. Sadtler and A. P. Alivisatos, *Nano Lett.* **8** (2008) 2551–2555.

22. T. T. Zhuang, F. J. Fan, M. Gong and S. H. Yu, *Chem. Commun* **48** (2012) 9762–9764.

23. P. Reiss, M. Protiere and L. Li, *Core/Shell Semiconductor Nanocrystals* **2** (2009) 154–168.

24. T. Serrano, I. Gómez, R. Colás, and J. Cavazos, *Colloids and Surfaces A: Physicochem. Eng. Aspects*, **338** (2009) 20–24

25. M. L. Curri, A. Agostiano, M. Catalano, L. Chiavarone, V. Spagnolo and M. Lugarå, *J. Phys. Chem.* **104** (2000) 8391-8397.

26. Kumar and A. Jakhmola, *Langmuir* **23** (2007) 2915-2918.

27. S. Wang and S. Yang, *Langmuir* **16** (2000) 389-397.

28. A. Kumar and A. Jakhmola, *Journal of Colloid and Interface Science* **297** (2006) 607–617.

29. M.V. Kovalenko, R.D. Schaller, D. Jarzab, M.A. Loi, and D.V.d Talapin, *J. Am. Chem. Soc.* **134** (2012) 2457-2460.

30. S. Trasatti, in *Electrified Interfaces in Physics, Chemistry and Biology, edited by R. Guidelli Kluwer Academic, Dordrecht,* (1992) pp. 229–244.

31. S. N. Inamdar, P. P. Ingole, and S. K. Haram, *Chem.Phys.Chem* (2008) **9** 2574–2579.

32. S. Haram, A. Kshirsagar, Y. Gujarathi, P. Ingole, O. Nene, J. Markad, and S. Nanavati, *J. Phys. Chem. C* **115** (2011) 6243–6249.

33. Y. Bae, N. Myung, and A. Bard, *J. Nano Lett.* **4** (2004) 1153–1161.

34. X. Zhao and X. Zhan, *Chem. Soc. Rev.* **40** (2011) 3728-3743.

35. A. Balan, D. Baran and L. Toppare, *Polym. Chem.*, **2** (2011) 1029-1043.

36. A. Cordones, M. Scheele, P. Alivisatos, and S. Leone, *J. Am. Chem. Soc.* **134** (2012) 18366-18373.

37. E. Kucur, Riegler, G. Urban, and T. Nann, *J. Chem. Phys.* **119** (2003) 2333